Journal of Hydrology 529 (2015) 511–523

Contents lists available at ScienceDirect

Journal of Hydrology

journal homepage: www.elsevier.com/locate/jhydrol

Reconstructing streamflow variation of the Baker River from tree-rings in Northern Patagonia since 1765

Antonio Lara [a,b,c,*], Alejandra Bahamondez [a], Alvaro González-Reyes [d,e], Ariel A. Muñoz [f,g,h], Emilio Cuq [a], Carolina Ruiz-Gómez [a]

[a] Laboratorio de Dendrocronología y Cambio Global, Instituto de Conservación, Biodiversidad y Territorio, Universidad Austral de Chile, Casilla 567, Valdivia, Chile
[b] Center for Climate and Resilience Research (CR)^2, Chile
[c] Fundación Centro de los Bosques Nativos FORECOS, Chile
[d] Departamento de Geología, Facultad de Ciencias Físicas y Matemáticas, Universidad de Chile, Santiago, Chile
[e] Advanced Mining Technology Centre (AMTC), Facultad de Ciencias Físicas y Matemáticas, Universidad de Chile, Santiago, Chile
[f] Instituto de Geografía, Pontificia Universidad Católica de Valparaíso, Valparaíso, Chile
[g] Centro de Tecnologías Ambientales (CETAM), Universidad Técnica Federico Santa María, Valparaíso, Chile
[h] Centro de Estudios Ambientales (CEAM), Universidad Austral de Chile, Valdivia, Chile

ARTICLE INFO

Article history:
Available online 16 December 2014

Keywords:
Water resources
Climate variability
Southern Annular Mode
Nothofagus pumilio
Chile
Argentina

SUMMARY

The understanding of the long-term variation of large rivers streamflow with a high economic and social relevance is necessary in order to improve the planning and management of water resources in different regions of the world. The Baker River has the highest mean discharge of those draining both slopes of the Andes South of 20°S and it is among the six rivers with the highest mean streamflow in the Pacific domain of South America (1100 $m^3 s^{-1}$ at its outlet). It drains an international basin of 29,000 km^2 shared by Chile and Argentina and has a high ecologic and economic value including conservation, tourism, recreational fishing, and projected hydropower. This study reconstructs the austral summer – early fall (January–April) streamflow for the Baker River from *Nothofagus pumilio* tree-rings for the period 1765–2004. Summer streamflow represents 45.2% of the annual discharge. The regression model for the period (1961–2004) explains 54% of the variance of the Baker River streamflow ($R^2_{adj} = 0.54$). The most significant temporal pattern in the record is the sustained decline since the 1980s ($\tau = -0.633$, $p = 1.0144 * 10^{-5}$ for the 1985–2004 period), which is unprecedented since 1765. The Correlation of the Baker streamflow with the November–April observed Southern Annular Mode (SAM) is significant (1961–2004, $r = -0.55$, $p < 0.001$). The Baker record is also correlated with the available SAM tree-ring reconstruction based on other species when both series are filtered with a 25-year spline and detrended (1765–2004, $r = -0.41$, $p < 0.01$), emphasizing SAM as the main climatic forcing of the Baker streamflow. Three of the five summers with the highest streamflow in the entire reconstructed record occurred after the 1950s (1977, 1958 and 1959). The causes of this high streamflow events are not yet clear and cannot be associated with the reported recent increase in the frequency of glacial-lake outburst floods (GLOFs). The decreasing trend in the observed and reconstructed streamflow of the Baker River documented here for the 1980–2004 period is consistent with precipitation decrease associated with the SAM. Conversely, other studies have reported an increase of summer streamflow for a portion of the Baker River for the 1994–2008 period, explained by ice melt associated with temperature increase and glacier retreat and thinning.

Future research should consider the development of new tree-ring reconstructions to increase the geographic range and to cover the last 1000 or more years using long-lived species (e.g. *Fitzroya cupressoides* and *Pilgerodendron uviferum*). Expanding the network and quality of instrumental weather, streamflow and other monitoring stations as well as the study and modeling of the complex hydrological processes in the Baker basin are necessary. This should be the basis for planning, policy design and decision making regarding water resources in the Baker basin.

* Corresponding author at: Instituto de Conservación, Biodiversidad y Territorio, Universidad Austral de Chile, Casilla 567, Valdivia, Chile. Tel.: +56 (63) 2221566, 2221228.
E-mail addresses: antoniolara@uach.cl (A. Lara), alejandra.bahamondez@gmail.com (A. Bahamondez), allitogonzalez@gmail.com (A. González-Reyes), arimunoz82@gmail.com (A.A. Muñoz), dencrono@uach.cl (E. Cuq), caroruizgomez@gmail.com (C. Ruiz-Gómez).

http://dx.doi.org/10.1016/j.jhydrol.2014.12.007
0022-1694/

1. Introduction

Water availability is a main limitation to future economic and social development in the different regions of the planet (Arnell et al., 2001; Viviroli et al., 2003). Changes in water availability due to climatic fluctuations as well as to an increase in water demand has raised the interest in understanding the susceptibility of agriculture, industry, hydroelectricity and domestic use to these variations (Meko and Woodhouse, 2011). This situation applies even to areas of relatively high annual rainfall, such as Northern Patagonia (40° – 48°S) in Chile under a rainy temperate climate (Dussaillant et al., 2012; Lara et al., 2003).

Instrumental precipitation and streamflow records in Chile located between 37° and 46°S show a dominant decreasing trend since the 1950s (Pezoa, 2003; Rubio-Álvarez and McPhee, 2010), and this area has experienced an estimated 30% precipitation decrease for the 1900–1999 period (Intergovernmental Panel on Climate Change, 2001). Regional climate models predict that this trend will continue in the region as well as in central Chile, especially during the austral summer (December–February, DGF, 2007). Limitations in water availability have been intensified by an increase in water demand in recent decades (Lara et al., 2003). These trends stress the importance of understanding the long-term variability of precipitation and streamflow, beyond the available instrumental records that in most cases start in 1950 and have limited quality, as well as geographic and elevation coverage (Dussaillant et al., 2012; Rubio-Álvarez and McPhee, 2010).

Tree-ring records provide continuous, annually-resolved series of past environmental changes for the last several centuries and in some cases, millennia. Long reconstructions can be developed by correlating tree-growth records with discharge and their variability may be analyzed at several frequencies. Reconstructions of streamflow from tree rings have been extensively used in North America to document and understand long-term trends in water availability (e.g. Brito-Castillo et al., 2003; Jain et al., 2002; Meko et al., 2007; Woodhouse, 2001; Woodhouse and Lukas, 2006). However, few streamflow reconstructions have been developed in South America, three of them in Argentina, for the Atuel River in Mendoza and for the Limay and Neuquén Rivers (Cobos and Boninsegna, 1983; Holmes et al., 1979; Mundo et al., 2012). In Chile two tree-ring streamflow reconstructions have been recently developed. One for the Puelo River (41° 35′S) and the other one for the Maule River (35° 40′S), both covering the last 400 years. (Lara et al., 2008; Urrutia et al., 2011). These reconstructions have improved the understanding of streamflow temporal and spatial patterns and their climatic forcings along the north–south hydroclimate gradient in the Pacific domain of Southern South America from Mediterranean-type to rainy temperate climates. Therefore, it is necessary to expand the latitudinal range of streamflow reconstructions, in order to enhance the knowledge of long-term discharge variability in Southern South America.

The understanding of the long-term variation of large rivers streamflow with a high economic and social relevance is necessary in order to improve the planning and management of water resources in different regions of the world. The Baker River has the highest mean discharge of those draining both slopes of the Andes South of 20°S and it is among the five rivers with the highest mean streamflow in the Pacific domain of South America (recorded mean annual streamflow 945 $m^3 s^{-1}$ at the Baker at the junction with Ñadis River gauge station and estimated at 1100 $m^3 s^{-1}$ at its outlet, Dussaillant et al., 2012).

Four other rivers draining to the Pacific that have a higher mean streamflow than the Baker are located in Colombia and one in Ecuador (Montaño and Sanfeliu, 2008; Sánchez et al., 2010). The Baker River drains a basin of 29,000 km^2 shared by Chile and Argentina. Both countries signed a Treaty on the Environment that includes the Protocol on Shared Water Resources. This protocol is oriented to cooperate and coordinate activities towards the protection, conservation and sustainable use of hydrological resources through the concept of integrated watershed management according to General Plans of Water Use for specific watersheds. Nevertheless, the Protocol does not establish compulsory or mandatory actions to any of its parts and it does not include conflict resolution procedures or obligations (Pardo, 2008). The Baker River is internationally known due to its high ecologic and economic value including conservation, tourism, recreational fishing, and projected hydropower from possible construction of 2 dams for the generation of 1020 Mw/h. The future of this project is uncertain due to the social conflict that it has raised, involving several international organizations and broad public attention (Dussaillant et al., 2012; Vince, 2009).

The main objective of this study was to develop a tree-ring reconstruction of the Baker River streamflow, expanding the short available instrumental records starting in 1961. The second objective was to understand the long-term temporal variability of the Baker River discharge from the interannual to the multi-decadal scales. The third objective was to identify the main large-scale atmospheric circulation and climatic forcings influencing river discharge of this southern river compared to the ones already analyzed in Southern South America.

2. Methods

2.1. Study area

The Baker River drains an international basin located between 46° and 48°S, that covers 29,286 km^2, mainly in Chile. It also includes 9013 km^2 in Argentina (30.8% of the basin (Fig. 1). The western portion of the watershed is formed by the Northern Patagonian Ice Field (NPIF). The North and North eastern portion of the basin is characterized by Lake General Carrera or Buenos Aires (local names in Chile and Argentina, respectively), that covers an area of 1850 km^2, being the second largest lake in South America. The main land use land cover types in the Baker basin determined from the GIS data provided by CONAF et al. (1999) are shrublands and grasslands (42% of the total), native forests (19% of the total, almost all forests located in Chile), barren lands located above-treeline (14%), (NPIF) and associated glaciers (3.1%).

The watershed flows towards the South-West and the outlet is in Bajo Pisagua at the Baker Fjord (Fig. 1). The main tributaries to the Baker (all of which have mean flows at least one order of magnitude smaller than the main stem) are the Nef, Colonia and Ventisqueros coming from the NPIF on the western side, and Chacabuco, Cochrane, Del Salto and Ñadis draining from the East (Dussaillant et al., 2012). Glacial-lake outburst floods (GLOFs) occur in the Colonia valley and have started to be studied in recent years. An increase in the occurrence of GLOF events has been reported. Several occurred in 2008 and 2009 (fall, spring and summer) and caused rapid floods constituting important hazards in the Baker valley (Dussaillant et al., 2009).

The geology of the Baker basin is dominated by the metamorphic rocks of upper Paleozoic age, as well as by different volcanic pyroclastic materials (Pino, 1976). Pleistocene glacial dynamics has driven most of the geomorphologic evolution of the Baker basin which has been overprinted by fluvial dynamics, landslides and volcanism due to Hudson volcano activity during the Holocene. The inner terminal moraine system of Lake General Carrera, was dated between 23 and 16 ky BP and therefore they can be associated with the Last Glacial Maximum (Kaplan et al., 2004).

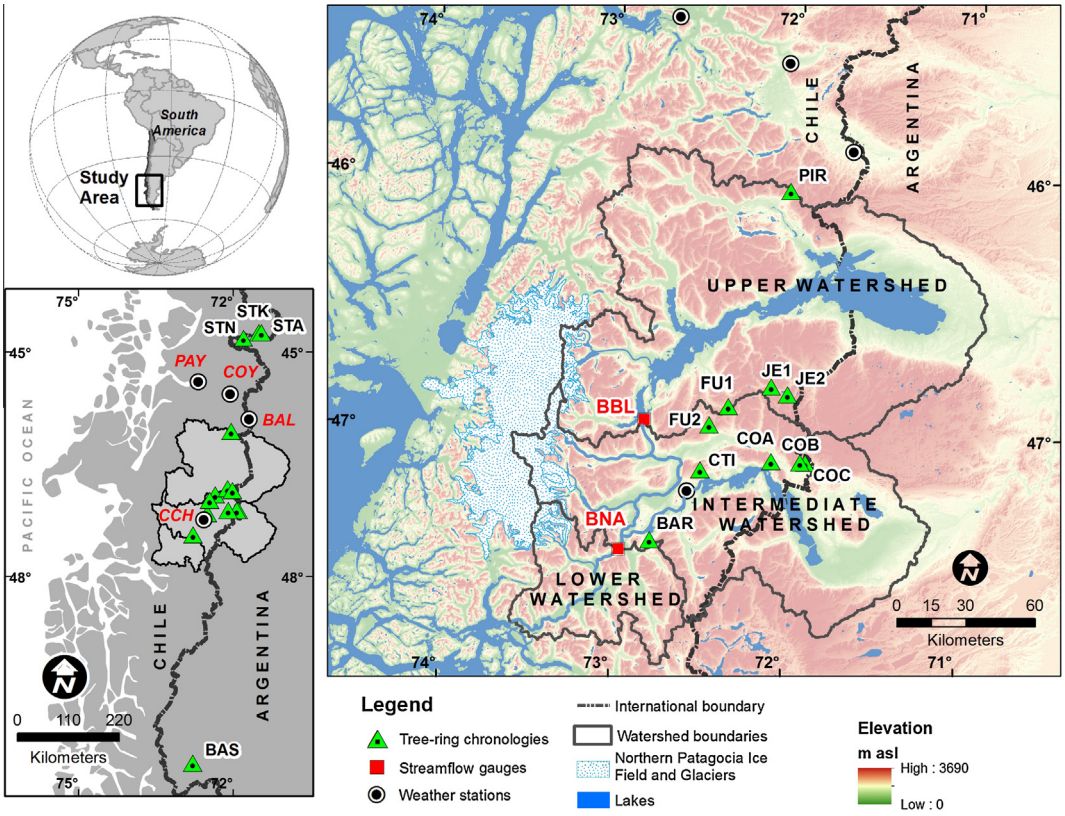

Fig. 1. Map of the Baker basin indicating the location of the tree-ring chronologies, meteorological and streamflow gauge stations. Codes for streamflow gauges: BBL: Baker at Bertrand Lake, BNA: Baker Bajo Ñadis. See Tables 1 and 2 for the codes of meteorological stations and chronologies.

Due to the rainshadow effect of the Andean Cordillera, annual precipitation varies from 2789 mm/year at Puerto Aysén on the western fjords, increases to an estimated value of 5000–10,000 mm/year on the Northern Patagonian Ice Field (Garreaud et al., 2013; Miller, 1976) and decreases towards the East to 740 and 270 mm/year in Cochrane and Chile Chico, the latter located on the south shore of Lake General Carrera (Dirección Meteorológica de Chile, DMC, and Dirección de Aguas, DGA, unpublished records; Fig. 1 for locations, and Table 1 for elevations). The mean austral summer (January) temperatures for Puerto Aysén and Balmaceda are 14.1 °C and 12.1 °C respectively and the mean austral winter (July) are 4.3 °C and 0.6 °C respectively (DMC unpublished records). Precipitation is concentrated in the winter season and decreases during the spring – summer (37% of annual precipitation between October and March for Cochrane). The Southern Annular Mode (SAM) is the main climate forcing in the region that determines the interannual variability of precipitation, with a smaller influence of El Niño Southern Oscillation (ENSO, Aravena and Luckman, 2009; Garreaud et al., 2009; Thompson et al., 2011).

2.2. Streamflow records

Streamflow monthly records from the Baker watershed were obtained from Dirección General de Aguas (DGA). These records were previously homogenized, validated and completed for missing data using regression on the closest comparable records following the methods proposed by Rosenblüth et al. (1997) and Rubio-Álvarez and McPhee (2010). None of the streamflow gauges has been affected by hydropower generation, irrigation channels or any other diversions. The records that would be suitable for reconstruction due to their length, completeness and percentage of the total streamflow of the Baker River that they represent came from the gauges at the outlet of Bertrand Lake (BBL, upper Baker basin), and the Baker at the junction with Ñadis River (BNA). A third candidate for reconstruction was defined by subtracting the records from both gauges. The difference represents the streamflow out of the intermediate Baker basin (Fig. 1).

The hydrologic year was defined starting in August (winter) when streamflow reaches its lowest value, with a maximum in summer (December through March) during the snowmelt season, and decreases until July of the next year, completing the annual cycle of discharge and recharge (Fig 2). This hydrological regime may be defined as nival with glacial contributions and is similar to the one described for the upper Baker watershed that goes from October through September with a maximum in February (Krögh et al., 2014). This delay in the seasonality compared to the

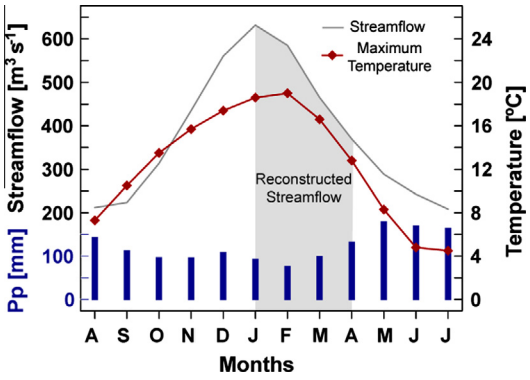

Fig. 2. Monthly precipitation and streamflow variation through the hydrologic year of the Baker River for the intermediate watershed (mean values for 1961–2004) indicating the reconstructed period.

intermediate watershed may be explained due to the water storage effect of Lake General Carrera (or Buenos Aires) that is stronger for the upper than for the intermediate watershed. The hydrologic year of the Baker differs from the one that characterizes the rivers in Central and South-Central Chile that goes from April to March of the following year.

2.3. Tree-ring records

The species selected for the reconstruction of the Baker River streamflow was *Nothofagus pumilio* (lenga). This deciduous species grows in Chile and Argentina between 36° 30′ and 55° 31′S and often dominates the upper tree line of the Andes. Increment cores from living trees used in this study were collected in 1997, 2008 and 2009 from a total of 14 sites, 10 of them located within the Baker watershed. The sites encompass old-growth dense stands and Krummholz stands at or near tree-line (Fig. 1). Sampling considered the entire range of site conditions where *N. pumilio* grows in the Baker basin along the West-East precipitation and North–South gradients within the basin. Using our knowledge of the variability in *N. pumilio* climate response (e.g. Aravena et al., 2002, Lara et al., 2005), we broaden the range of sites, and we include four additional sites in Chile and one in Argentina located outside the Baker Basin (Fig. 1). Forest stands selected for sampling were not disturbed or little disturbed by human causes such as logging or fire, as well as by natural disturbances.

Tree-ring series from highly correlated site chronologies were grouped into five composite chronologies, four in Chile and one in Argentina, the latter formed by only one site chronology. The characteristics of the tree-ring chronologies and sites that are included in each composite chronology are described in Table 2.

Two radii from each living tree were collected in each of these sites. Cores and sections were sanded, and tree-rings were measured under a microscope to the nearest 0.001 mm, cross-dated and standardized using standard dendrochronological techniques (Fritts, 1976; Holmes, 1983; Stokes and Smiley, 1968; Robinson and Evans, 1980). The computer program COFECHA (Holmes, 1983) was used to detect measurement and cross-dating errors. For dating purposes, we followed Schulman's convention (1956) for the Southern Hemisphere, which assigns to each tree ring the date of the year in which radial growth started. Cross-dating verifies the assignment of a calendar year to each ring in every sample by comparing the growth patterns among the different cores and sections. Cross synchronization of annual ring width patterns backward from the outer ring on radii collected from living trees, and then the assignment of exact calendar years is achieved among a large sample of trees and cores. The accuracy of the first master chronology in an area is then tested (and ultimately validated if no disagreements are discovered) upon comparison with every additional dated series. Standardization removes non-climatic variability from tree-ring series, such as the typical decline in ring width due to the increase in age and circumference of trees (Fritts, 1976). In order to preserve a large percentage of the low-frequency variance, standardization was accomplished by fitting each ring-width series to a negative exponential or linear regression curves, using the TURBO ARSTAN program (Cook, 1985; Cook et al., 2007). Regional chronologies were developed by combining all the radii of the individual sites included in each composite.

The quality of the tree-ring chronologies was assessed using running series of Rbar and Expressed Population Signal (EPS) statistics using a 50-year window with a 25-year overlap (Briffa, 1995). Rbar is the mean correlation coefficient of all possible pairings among tree-ring series from individual cores, for a common time interval (Briffa, 1995). EPS is a measure of the correlation between the average of a finite number of tree-ring series and a hypothetical chronology that has been infinitely replicated, and assumed to represent the population (Briffa, 1995).

2.4. Tree-ring reconstruction

In order to identify the relationships between streamflow and tree growth, we computed the correlations between tree-ring width indices from the composite chronologies and monthly mean departures from the Baker River intermediate watershed. We tried various monthly and seasonal combinations of the three available streamflow records that were candidates for reconstruction (BLB, BNA and BNA–BLB), following the methods described by Fritts (1976) and Blasing et al. (1984).

Reconstruction equations were estimated by regressing monthly streamflow departures on principal components (PCs) extracted from the four tree ring composite chronologies and one individual site. Three PCs were used as candidate predictors. A stepwise multiple regression model was applied to develop the Baker streamflow reconstruction. The entire common period (1961–2004) of the composite streamflow record was used to calibrate the tree-ring model utilizing the "leave-one-out" cross-validation procedure (Meko, 1997; Michaelsen, 1987). In this method each observation is successively withdrawn; a model is estimated on the remaining observations, and a prediction is made for the omitted observation. The proportion of variance explained by the regression or adjusted R^2 (R^2_{adj}) was used to evaluate the quality of fit between the observed and predicted values. *F*-value of the regression, reduction of error (RE), the Durbin–Watson test (Ostrom, 1990) and other statistics were used to assess the robustness of reconstruction model.

2.5. Temporal and spatial variability

Singular Spectral Analysis was used to identify the dominant periods at which variance occurs in the streamflow reconstruction and other time series (Vautard and Ghil, 1989). We used the Multi-Taper Method (MTM; Mann and Lees, 1996) to identify the cycles that explain significant proportions of variance. In addition, to allow a simultaneous representation of the dominant modes of variability in the reconstruction and their variations and significances through time, a Continuous Wavelet Transform and cross wavelet analysis was developed (Grinsted et al., 2004; Torrence and Compo, 1998).

We applied the Mann–Kendall test Kendall (1975) for the assessment of tendencies in the reconstructed Baker streamflow record considering a slope equal to zero (i.e. no trend) as the null-hypothesis. Mann Kendall is a non-parametrical test that analyzes trends in time series. In addition, the Mann–Kendall test has been selected as one of the most robust statistical tools for the detection of linear trends in environmental data sets (Hess et al., 2001). Nevertheless, this and other methods are restricted by the difficulty in determining the null-hypothesis and the reduction of significance in statistical testing due to long-term persistence in hydroclimatic instrumental and proxy records (Cohn and Lins, 2005; Koutsoyiannis and Montanari, 2007).

Sea level pressure (SLP) across the Pacific and Atlantic Oceans were compared with the Baker observed and reconstructed streamflow to determine the atmospheric and oceanic features more closely related to discharge variations. For this analysis we used Gridded (2.5° × 2.5°) mean monthly SLP time series from the NCEP–NCAR Reanalysis global database (Kistler et al., 2001 and updates) (http://www.cdc.noaa.gov/Correlation/). We used linear correlation and mapping routines available at the KNMI (Royal Netherlands Meteorological Institute) available at the Climate Explorer Website (http://climexp.knmi.nl/).

2.6. Climatic forcings

Pearson's temporal correlation coefficients between the annual reconstruction and indices of atmospheric circulation, such as ENSO, expressed as the Southern Oscillation Index (SOI, http://www.cru.uea.ac.uk/cru/data/soi.htm), the Pacific Decadal Oscillation (PDO, http://jisao.washington.edu/pdo/PDO.latest) and the Southern Annular Mode (SAM) or Antarctic Oscillation (AAO, http://jisao.washington.edu/data/aao/slp/) were evaluated to identify the major climatic forcings affecting interannual or decadal to multidecadal variations in the Baker River streamflow. Temporal correlations between monthly and seasonal observed streamflow and these indices were especially evaluated to identify possible effects of these forcings on discharge. Additionally, we analyzed the long-term relation of the reconstructed Baker streamflow with reconstructions of the PDO (Biondi et al., 2001) and SAM (Villalba et al., 2012) based on tree-ring records.

3. Results and discussion

3.1. Tree-ring records

Mean sensitivity of the various composite chronologies, characterizing the year-to-year variability in tree-ring records (Fritts, 1976), ranges between 0.167 and 0.247 (Table 3). These values are within the range of those reported for the species along its complete latitudinal gradient (mean sensitivity 0.15–0.28, Lara et al., 2005). The mean Rbar for the different composite chronologies, representing the mean correlation among tree-ring series for overlapping 50-year periods, varies between 0.311 and 0.355 (Table 3). These values are higher than those reported earlier for *N. pumilio* except for one composite chronology (Lara et al., 2005). First order autocorrelation in each of the chronologies ranges between 0.49 and 0.69 (not shown). All the chronologies have at least 5 radii covering the period since 1782. The EPS value is above 0.85 starting between 1765 and 1800, with the exception of Jeinimeni, which reaches this threshold in 1820 (Table 3). EPS values above or close to 0.85 suggest temporal stability, good quality and a strong common signal in the time series (Wigley et al., 1984).

Tree-ring growth patterns for the various chronologies show both inter-annual as well as low-frequency variations (Fig. 3). The composite chronologies have similar high-frequency patterns as indicated by the correlation among them. Correlation coefficients (r) vary between 0.25 and 0.58 ($p < 0.001$ in all cases), Table S1, Supplementary Material). All the tree-ring records show a period below the mean centered in 1812–1816 (Fig. 3). In the recent portion of the chronologies, Cisnes, Furioso and Calafate show a decreasing trend since the 1990s and this decline is especially steep in Furioso (Fig. 3). Conversely, Oportus and Jeinimeni growth is above the mean without a clear trend in the same period. The three principal components PC1, PC2 and PC3 explain 29.9%, 28.1% and 22.0% of the variance in tree-growth, respectively. The relatively even distribution among the variance explained by the different PCs can be associated with the dominant response of *N. pumilio* tree-growth to temperature or precipitation according to the location of the chronology sites along a broad West to East and North to South environmental gradient. Similar variability in *N. pumilio* growth response to climate has been documented (Aravena et al., 2002; Lara et al., 2005). Examples of the correlation between selected composite chronologies with precipitation and temperature records are included in Supplementary Material.

PC1 and PC3 loadings are dominated by chronologies at year t, whereas loadings of PC2 are dominated by Furioso and Calafate lagged chronologies (Supplementary Material). This may be explained by the typical tree-growth response of *N. pumilio* that has demonstrated to be determined by both the climate conditions of the current and previous growing seasons (Villalba et al., 2003, Aravena et al., 2002). The latter study developed a reconstruction of minimum temperature of southern Chilean Patagonia (51° – 55°S) modeling climate as a function of tree-growth in the current and previous years. This is consistent with the knowledge that tree-growth of different species may depend on the climate of not only the current year but of the previous one or more years (Fritts, 1976).

3.2. Streamflow reconstruction

Based on the correlation functions between the tree ring composite chronologies and the principal components extracted from

Table 1
Meteorological stations used for developing regional precipitation and maximum temperature time series. Station locations are indicated in Fig. 1.

Station name	Code	Variable[a]	Elevation (m asl)	Period	Missing values (%)	
					Pp	Tx
Balmaceda	BAL	Pp, Tx	520	1961–2005	0	0
Coyhaique	COY	Pp, Tx	300	1961–2005	0	0.5
Puerto Aysén	PAY	Pp	10	1961–2005	1.1	
Cochrane	CCH	Tx	215	1970–2005		2.3

[a] Pp = monthly precipitation, Tx = maximum temperature (monthly average).

Table 2
Site characteristics of tree-ring records included in the composite chronologies.

Composite chronologies (Code)	Site chronologies	Code	Period	Latitude (W)	Longitude (S)	Elevation (m asl)
Cisne (CIS)	Santa Teresa Abajo	STA	1784–1997	−44.73	−71.50	1000
	Santa Teresa Krummholz	STK	1770–1997	−44.73	−71.45	1200
	Santa Teresa Nueva	STN	1765–2008	−44.74	−71.94	1020
Oportus (OPO)	Cerro Oportus B	COB	1764–1997	−47.13	−71.90	1080
	Cerro Oportus C	COC	1739–1997	−47.13	−71.93	1120
	Cerro Oportus A	COA	1759–2009	−47.13	−72.10	1160
	Portezuelo Ibañez	PIR	1712–2008	−46.07	−72.04	1180
Jeinimeni (JEI)	Jeinimeni 1	JE1	1858–2002	−46.84	−72.11	1070
	Jeinimeni 2	JE2	1690–2009	−46.87	−72.02	1040
Furioso (FUR)	Barrancoso	BAR	1836–1997	−47.45	−72.78	900
	Furioso Krummholz	FU1	1868–1997	−46.92	−72.35	1170
	Cerro Tamango Inferior	CTI	1750–1997	−47.17	−72.50	960
	Furioso 2	FU2	1722–2008	−46.99	−72.46	1060
Calafate (CAL)	Cerro Buenos Aires	BAS	1741–2009	−50.36	−72.79	840

Table 3
Descriptive statistics for the composite standard chronologies.

Chronologies	Period	N° of radii	Starting year with ⩾5 radii	Mean sensitivity[a]	Mean Rbar[b]	Year of EPS[c] ⩾ 0.85	Variance explained by the first Eigenvector (%)
Cisne	1765–2008	50	1779	0.209	0.345	1800	57.58
Oportus	1712–2009	291	1747	0.167	0.318	1765	25.56
Jeinimeni	1690–2009	54	1782	0.217	0.311	1820	33.77
Furioso	1722–2008	67	1724	0.247	0.355	1767	60.18
Calafate	1741–2009	104	1764	0.206	0.352	1800	31.53

[a] Mean sensitivity is the measure of the relative changes in ring width variations from year to year (Fritts, 1976).
[b] Rbar is the mean correlation coefficient for all possible pairings among tree-ring series from individual cores, computed for a specific common time interval. In this case we used a 50-year window with a 25-year overlap (Briffa, 1995).
[c] Expressed Population Signal (EPS) statistic for the composite chronologies using a 50-year window with 25-year overlap. EPS threshold fixed at 0.85 is considered adequate to reflect a reliable common growth signal (Wigley et al., 1984).

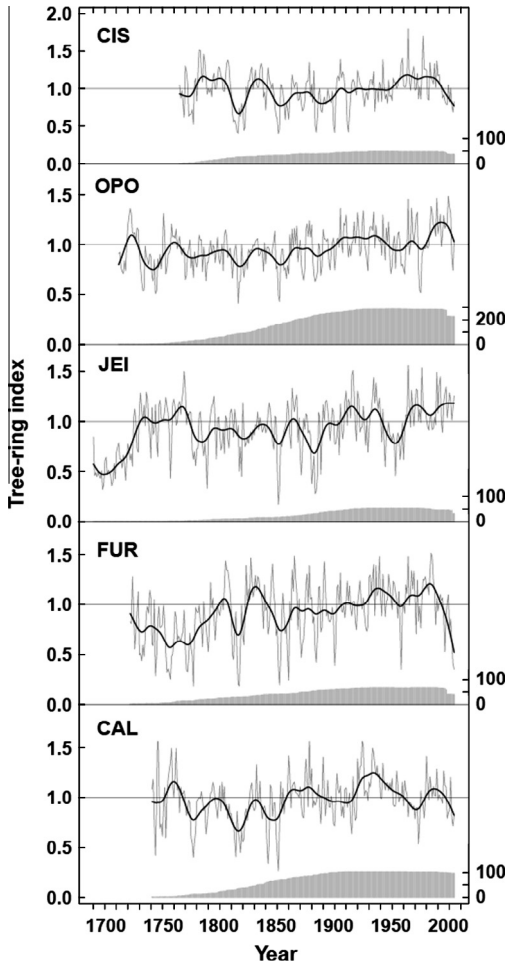

Fig. 3. Standard tree-ring composite chronologies of *Nothofagus pumilio*. Tree-ring indices provide nondimensional values that show changes in radial growth over time. The chronologies are also shown with a cubic spline designed to reduce 50% of the variance in a sine wave with a periodicity of 25 years (Cook and Peters, 1981). Sample size is shown as a shaded area at the bottom of each chronology, representing the total number of tree-ring series per year.

them and the monthly mean departures from the Baker River streamflow instrumental records, the hydrological period from January to April (summer to early fall corresponding to the snowmelt season) was selected for the reconstruction. The shortest composite chronology started in 1765, and the Baker validated streamflow record covered the 1961–2004 period. Therefore, the period for reconstruction was defined as 1765–2004.

The reconstruction using the "leave-one out procedure" (Meko, 1997; Michaelsen, 1987) selected three predictors: PC1, PC2 and PC3 extracted from the composite chronologies. The reconstruction equation is:

$$SB_t = 513.048 + 30.656PC3_t - 14.892PC1_t + 15.077PC2_{t+2}$$

where SB_t is the predicted summer-early fall (January-April) streamflow for the Baker River for year t, and PC1, PC2, PC3 are the principal component amplitudes from the composite chronologies for the years indicated as t or $t+2$.

The regression model for the period (1961–2004) explains 54% of the variance of the Baker River streamflow expressed as (R^2_{adj} = 0.54, Table 4). This statistic is higher compared to the variance explained by previous streamflow reconstructions in Chile for the Puelo and Maule Rivers (R^2_{adj} = 0.42, and 0.43, respectively; Lara et al., 2008; Urrutia et al., 2011). The reduction of error statistic (RE = 0.49) is positive and indicates useful skill in the regressions (Gordon and Le Duc, 1981, Table 4). The Durbin–Watson statistic indicate that the residuals are not autocorrelated (Table 4). The residuals are randomly distributed, have no trend in the 1961–2004 period (slope 0.136, p = 0.74), and are not correlated with the predictors (Figs. S5–S8 in Supplementary Materials). The root-mean-square error (RMSE) is useful to estimate the error contained in the reconstruction as a proportion of the variable that is being reconstructed. The RMSE summer-early fall Baker River streamflow in the reconstruction is 36.64 $m^3 s^{-1}$, representing 7.1% of the mean reconstructed streamflow (513.3 $m^3 s^{-1}$). The estimate of error is based only on the calibration period (1961–2004), and the true uncertainty in the reconstruction is likely higher in the pre-instrumental period due to several factors such as decreasing sample size and temporal variability in the tree growth precipitation and temperature relationships, that control the reconstructed streamflow.

The mean January–April streamflow of the Baker River represents 45.2% of the mean annual streamflow in the entire hydrological year (Fig. 2). The mean summer streamflow of the intermediate basin reconstructed in this study represents 43% of the discharge at the Ñadis station (BNA, Fig. 1) that includes both the upper and the intermediate basins with a mean summer discharge of 1192 $m^3 s^{-1}$.

The predicted streamflow captures both high and low variations in the instrumental record as indicated by the similar differences

Table 4
Statistics computed for the tree-ring based reconstruction of the summer – early fall (January–April) streamflow for the Baker River.

Period	R^2	R^2_{adj}	F	P_f	SE	RE	RMSE	DW
1961–2004	0.56	0.54	16.74	0.0001	35.79	0.49	36.64	2.04

R^2 = square of the multiple correlation coefficient; R^2_{adj} = square of the multiple correlation coefficient adjusted for loss of degrees of freedom; F = F statistic; P_f = - probability value of the F statistic; SE = standard error; RE = reduction error; RMSE = root-mean-square error (measure of reconstruction uncertainty); DW = Durbin–Watson, statistic used to test for first-order autocorrelation of the regression residuals (Ostrom, 1990).

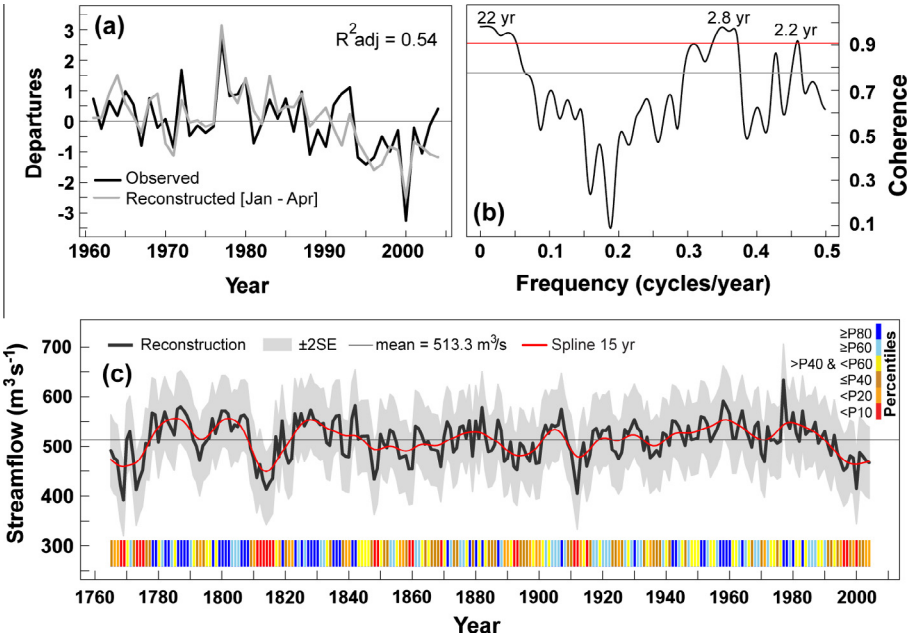

Fig. 4. (a) Observed and predicted mean austral summer to early fall season (January–April) departures of the Baker River streamflow between 1961 and 2004. (b) Coherence spectrum of the observed and predicted streamflow of the Baker River estimated for the 1961–2004 period. The grey and red horizontal lines indicate the 95% and 99% confidence limits, respectively. (c) January to April reconstruction of the lower watershed Baker River discharge for the period 1765–2004 ($m^3\ s^{-1}$). The gray shaded area indicates ±2 squared error of cross validation, and the horizontal line indicates the mean discharge for the 1765–2004 period. The color bands on the bottom represent the percentile distribution (<P10 to ⩾P80) obtained from the reconstruction series. Blue, yellow and red colors indicate years with high, average and low discharge compared to the mean value, respectively. (For interpretation of the references to color in this figure legend, the reader is referred to the web version of this article.)

between the observed and the predicted values for the positive and negative deviations (Fig. 4a). Coherency spectrum between the observed and predicted January – April streamflow of the Baker River, estimated over the 1961–2004 period shows common cycles (Fig. 4b). In general, the coherency spectra show fidelity in those bandwidths in both the observed and predicted time series. Oscillations centered in 22-year followed by 2.8 and 2.2 year periods are coherent for both series ($p < 0.01$) as an indication of synchrony at those time periods in both the observed and the predicted time series (Fig. 4b).

3.3. Temporal patterns

From the reconstructed values, we identified the years and periods of highest and lowest streamflows for Baker River since 1765 (Table 5). Three of the years among those with the highest streamflows occurred after 1950, with 1977 as the most extreme high-streamflow event in the entire record (3.06 SD above the mean), followed by 1958 and 1959 (Table 5).

Table 5
Ranking of the individual years, 5 and 10-year periods with extreme low and high values in the reconstructed Baker River streamflow.

Period	Lowest streamflow		Highest streamflow	
	Year	SD	Year	SD
1	1769	−3.09	1977	3.06
	1912	−2.75	1958	1.96
	1773	−2.56	1842	1.74
	1814	−2.53	1959	1.69
	2000	−2.48	1787	1.68
5	1812–1816	−2.01	1786–1790	1.35
	1765–1769	−1.59	1956–1960	1.28
	1996–2000	−1.44	1977–1981	1.27
	1772–1776	−1.43	1825–1829	1.13
	1911–1915	−1.37	1799–1803	1.12
10	1809–1818	−1.40	1781–1790	1.07
	1766–1775	−1.39	1799–1808	1.05
	1995–2004	−1.21	1824–1832	1.01
	1891–1900	−0.81	1951–1960	0.97
	1908–1917	−0.74	1977–1986	0.89

In terms of 10-year moving averages, there are two periods in the last decades among the five with the highest streamflow: 1951–1960 and 1977–1986. Two of the years with extreme low reconstructed discharge occurred early in the record (1769 and 1773, with −3.09 and −2.75 SD below the mean, respectively Table 5). Nevertheless, the events before 1800 need to be judged carefully since the chronologies used for the reconstruction have a lower replication. The decades with the lowest streamflow are 1809–1818 and 1766–1775, and they are also clearly shown in the reconstruction and in the periods of successive years that fall in the percentile <10 (Fig. 4c).

Tendency analysis using the Mann Kendal test (indicated by τ non-dimensional index) that identifies the periods where slope is significantly different from zero, indicated that 1980–2004 is the only 25-year period of reconstructed streamflow with a significant trend of any sign ($\tau = -0.633$, $p = 1.0144 * 10^{-5}$, Fig. 4c). The decreasing trend is also evident in the summer to early fall (January to April, Fig. 4a) and annual streamflow (not shown) instrumental records after 1980 (both series are highly correlated, $r = 0.71$, $p < 0.0001$).

Different waveforms were isolated from the streamflow reconstruction using Singular Spectral Analysis SSA (Vautard and Ghil, 1989; Fig. 5a). The spectral signal of the Baker reconstruction shows oscillations centered in 22.7, 9.4, 5.8, 5.1, 4.2, 3.8, 2.7 and 2.1 year-periods at various confidence levels for the 1765–2004 interval (Fig. 5a). The 21.2–28.5 year-cycle was identified as the most significant oscillatory mode, explaining 23% of the total variance. This interdecadal oscillation mode in the streamflow variability shows higher amplitude and is better structured from 1765 to 1830 (Fig. 5c). This is a common pattern to several proxy records across the Pacific basin, suggesting that interdecadal variations in the Pacific-related climate system were more conspicuous before the 20th century (Villalba et al., 2001). Other

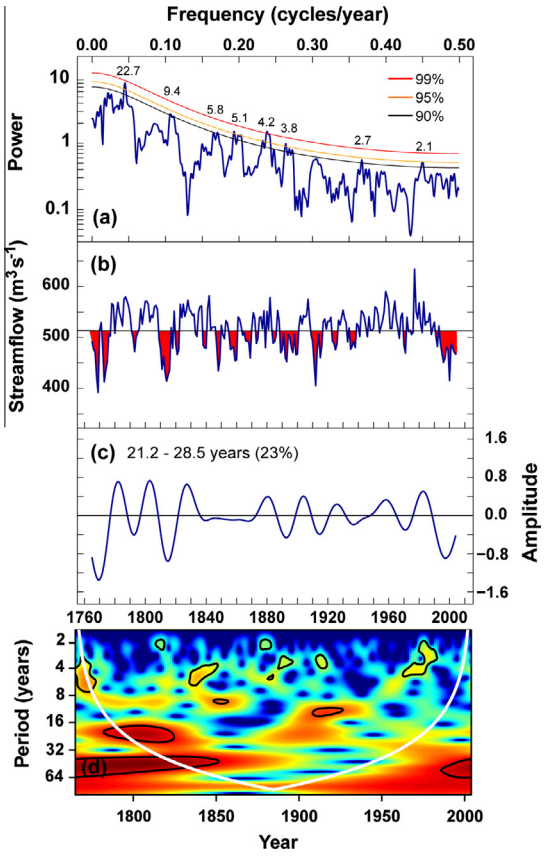

Fig. 5. (a) Spectral signal of the Baker River streamflow reconstruction from 1765 to 2004, with blue, orange and red lines indicating the 90%, 95% and 99% confidence limits, respectively. (b) Baker River streamflow reconstruction with the periods below the mean highlighted in red, to emphasize the low-frequency patterns. (c) Singular spectrum amplitude of the Baker River streamflow variations for a period of 21.2–28.5 years, identified as the most significant oscillation mode (23% of the total variance associated to this waveform). Units are dimensionless. (d) Power amplitude spectrum of the Continuous Wavelet Transform to detect spatial and temporal cycles on the Baker reconstruction, with the time scale slightly displaced compared to Panel (c). The thick black contours above the cone of influence designate the 95% confidence level against red noise. Within the cone of influence, edge effects become important. (For interpretation of the references to color in this figure legend, the reader is referred to the web version of this article.)

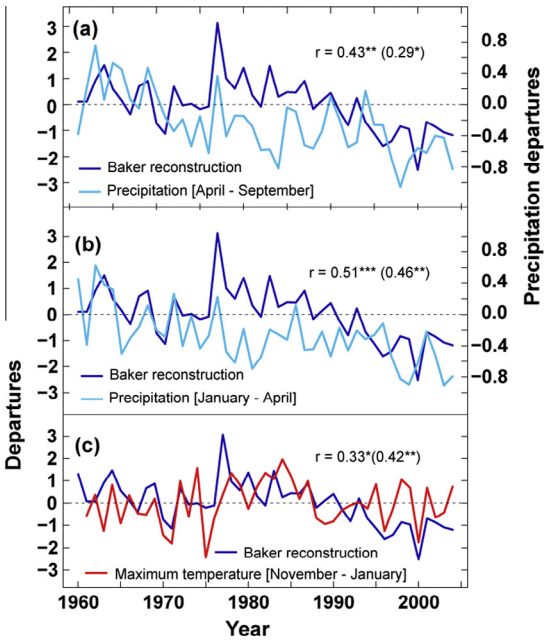

Fig. 6. (a) January–April reconstructed streamflow for Baker River and previous fall to early spring (April–September) regional precipitation for 1961–2004. (b) Reconstructed streamflow and current summer to early fall (January–April) regional precipitation. (c) Streamflow reconstruction and current summer (November-January) regional maximum temperature (monthly averages). Pearson correlation r in parentheses were calculated from pre-whitened series. Significance p levels are: *0.05, **0.01, ***0.001.

reconstructions such as those for the Maule and Puelo Rivers report similar although shorter cycles (17.5 and 19 years, 21 and 12% of explained variance respectively, Lara et al., 2008; Urrutia et al., 2011).

The negative amplitudes for a cycle of 21.2–28.5 years coincide with two periods of below the mean reconstructed streamflow (1766–1775 and 1809–1818, Fig. 5c, Table 5). Interestingly, the latter pattern coincides with the low-frequency signal identified in the wavelet analysis for a period of 16–32 years between 1800 and 1825 (Fig. 5b–d). The wavelet also shows a period longer than 32 years centered at 1840–1850, with a main portion below the cone of influence, probably as an indication of its lower strength (Fig. 5d). This is consistent with the absence of this decadal to multi-decadal departure in streamflow (Fig. 5b, c, and Table 5). The 2.1 and 2.7-cycles identified in this study for the instrumental period is similar to the 2.2–2.7-year cycle since the 1940s in the co-spectral analysis of the observed and predicted values in the Maule reconstruction (Urrutia et al., 2011).

3.4. Baker streamflow and climatic forcings

The Baker River reconstructed summer streamflow mainly responds to recorded regional precipitation in the previous fall, winter and spring (April to September) partially reflecting snow accumulation ($r = 0.43$, $p < 0.01$, Fig. 6a). This correlation is strongly influenced by the negative slope of both records and decreases when both series are pre-whitened ($r = 0.29$, $p < 0.05$). Streamflow is also correlated with current observed summer – early fall precipitation ($r = 0.51$, $p < 0.001$, and $r = 0.46$, $p < 0.01$ for the pre-whitened series, Fig. 6b). The regional precipitation record for both seasons has a significant negative trend over the 1961–2004 period as indicated by the Mann Kendall test ($p < 0.05$). The Baker streamflow record is also correlated with the regional maximum temperature of the spring and summer of the current hydrological year (November–January, $r = 0.33$, $p < 0.05$) as a snowmelt response. If the series are prewhitened, this correlation increases since the temperature record has no trend whereas the streamflow has a decreasing trend ($r = 0.42$, $p < 0.01$, Fig. 6c).

Differences in the seasonal correlations of the Baker River streamflow with recorded precipitation might indicate some importance of summer rainfall to streamflow in a nival dominated regime. Differences might also point to limitations of precipitation records at low elevations to capture snowfall. Low-elevation stations may underestimate basin rainfall because much of the basin lies at high elevations (Dussaillant et al., 2012; Krögh et al., 2014).

A recent publication (Krögh et al., 2014) used a modeling approach with daily records based on ERA-interim and CFSR reanalysis data in order to overcome the limitations of observed instrumental data for the upper Baker basin (Fig. 1). This study made an important contribution to the understanding of the hydrological processes that explain the observed Baker River streamflow record. Infiltration is documented as the main component of the water balance, accounting for 73% of the total precipitation (Krögh et al., 2014). The fact that the soil component is the dominant modulator of runoff, and that most occurs as slow interflow provides a sound explanation of how precipitation (rain and snow) falling in late fall, winter and spring (April through September) might supply the soil water that becomes available for trees

during the summer growing season (approximately November through March) and at the same time contributes to high summer to early fall flows (January–April, Fig. 6a). Water from summer precipitation (mainly rain) is also stored in the soil and available for trees, and contributes to summer streamflow (Fig. 6b). This provides a basis to understand how precipitation controls both tree-growth and streamflow and why tree-ring chronologies explain an important percentage of the Baker River streamflow variability.

Our results indicating that streamflow reduction in the last decades is mainly determined by a reduction in precipitation due to an increasing trend in SAM are consistent with the findings reported by Lenaerts et al. (2014). These authors report a slight atmospheric cooling at the upper North and South Patagonian Ice Fields as well as a small but insignificant increase in ice field Surface Mass Balance (SMB) for the period 1979–2012. This near neutral SMB might be an indication that the North Patagonic Ice Field (NPIF) is not making a significant contribution to the Baker streamflow that would modify its dependence on precipitation. Nevertheless, these results contradict a study reporting the significant increasing trend for the summer streamflow (January through March) for the period 1994–2008 inferred from the streamflow difference between two gauging stations in the Baker River (Mann Kendall test, $p < 0.02$ Dussaillant et al., 2012). This increase in the streamflow of this section of the Baker River has been associated to the contribution of the Nef Glacier and the NPIF as a consequence of ice melt due to temperature increase (Dussaillant et al., 2012), consistent with a generalized glacier retreat and thinning process reported for the NPIF (Aniya, 2007; Rivera et al., 2007).

The occurrence of the extreme high summer streamflow of 1977 recorded in both the instrumental and reconstructed time series is coherent with a significant positive departure in precipitation from the previous fall to spring seasons (April–September) that might increase snow accumulation, and to a maximum summer temperature value above the mean (Fig. 6a and b). The lack of instrumental discharge records before 1961 prevents the identification of the climatic factors that might explain the positive deviations of summer streamflow reconstructed for 1958 and 1959. Dussaillant et al. (2009) have developed a record of the glacial-lake outburst floods (GLOFs) in the Colonia tributary that produce extreme instantaneous peaks using Baker daily records as part of the evidence for their identification. Nevertheless, these dated events could not be discerned in the monthly or summer discharge instrumental records used in our study. Therefore, the causes of the occurrence of recent extreme high observed (1977) and reconstructed (1958, 1959, 1977) summer flows remain unclear.

The analysis of the atmospheric circulation patterns that might be influencing regional precipitation and therefore the observed discharge (December–March) as well as the reconstructed summer-early fall (January–April) streamflow of Baker River using gridded climatic data shows some clear patterns (Fig. 7a and b). Above mean observed streamflows are related to below-average sea level pressure (SLP) in December–March across the Pacific Ocean at 20° – 50°S, as indicated by the negative correlation values (Fig. 7a). Conversely, streamflow is positively correlated with SLP anomalies at latitudes 60° – 80°S. This contrasting pattern may be regarded as the main driver for positive anomalies of the observed Baker River summer streamflow that is determined by a northward displacement of the westerly winds and zonal flow throughout a large geographic area over the Pacific Ocean ranging between 150° and 70°W that bring precipitation to mid latitudes (Garreaud et al., 2013). The Puelo River summer-fall streamflow reconstruction responds to a similar atmospheric pattern described for the Baker River with negative correlation with SLP at mid-latitudes and positive correlation at high latitudes (Lara et al., 2008, Fig 7a and b).

We analyzed the correlation between the reconstructed Baker River discharge and the Southern Annular Mode SAM (also called

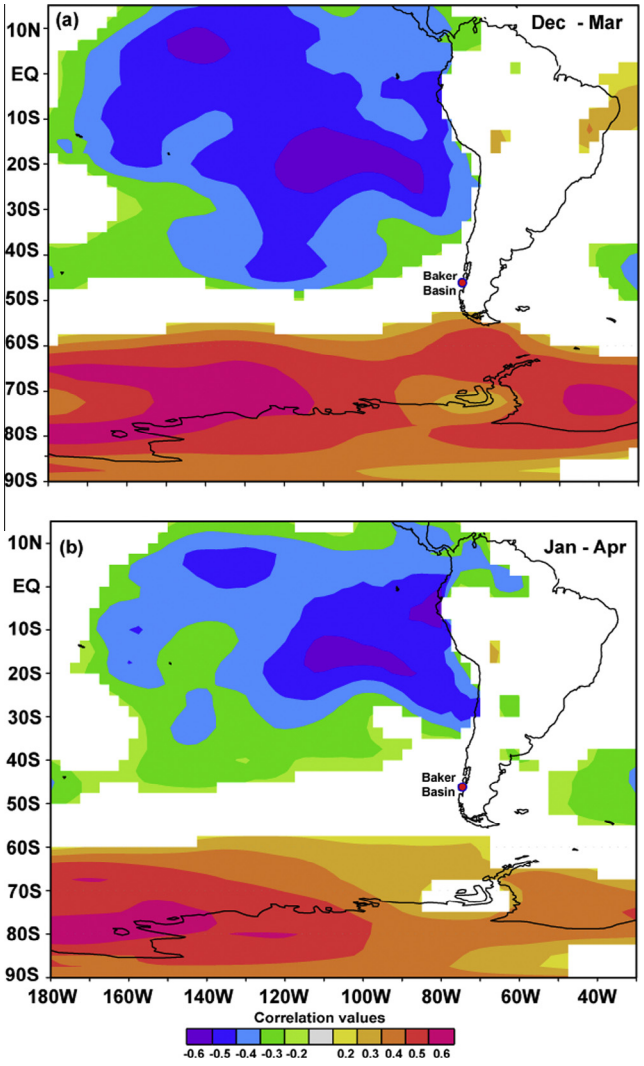

Fig. 7. Spatial correlation patterns estimated during the 1961–2004 interval between: (a) observed summer streamflow and sea level pressure (SLP) for December–March. (b) Same for reconstructed January–April streamflow. The red circle indicates the location of the Baker River basin. Critical Pearson correlation significant at 95% confidence level is $r = \pm 0.27$).

Antarctic Oscillation, AAO) (1961–2004), which is the dominant mode of climate variability at higher latitudes in the Southern Hemisphere (Thompson and Wallace, 2000). The SAM represents the meridional sea level pressure gradient between mid (40° – 45°S) and high latitudes (60° – 65°S) over the Pacific and the Atlantic Oceans. Positive departures of the Baker River instrumental summer streamflow are associated with the negative state of the late spring-early fall (November–April) SAM record developed by Marshall (2003) from instrumental data (designated as SAM-Marshall hereafter). There is a negative significant correlation between the Baker River and SAM-Marshall records ($r = -0.55$ $p < 0.001$ for the 1961–2004 for both the raw and the pre-whitened series, Fig. 8a). This correlation is even higher with the reconstructed streamflow ($r = -0.58$, $p < 0.001$ and $r = -0.46$, $p < 0.01$ for the pre-whitened series Fig. 8b). These correlations are consistent with the spatial patterns of SLP associated with the Baker streamflow (Fig. 7a and b).

A similar association of reconstructed streamflow and summer-fall SAM has been described for the Puelo River ($r = -0.45$, $p < 0.01$, 1947–1999, Lara et al., 2008). Interestingly, further north, the Maule River annual (April–March reconstructed streamflow

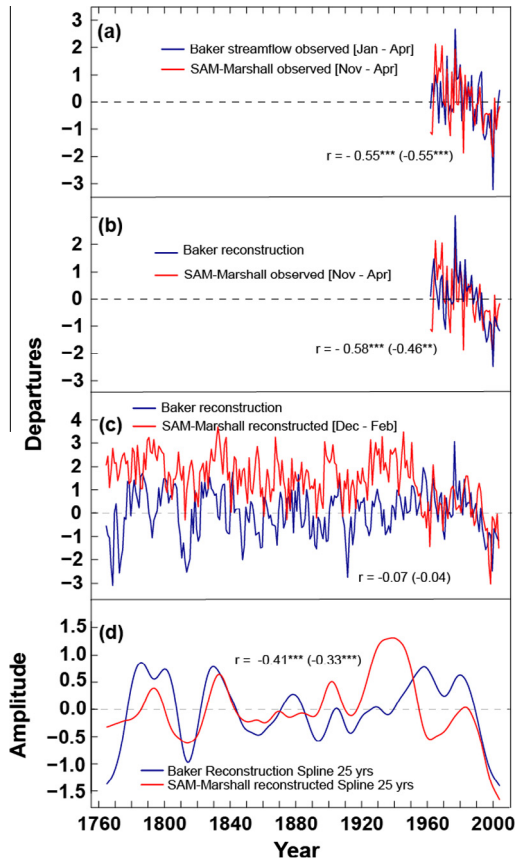

Fig. 8. (a) Observed Baker River streamflow and observed Southern Annular Mode (SAM-Marshall) for the 1961–2004 period. (b) Same for reconstructed streamflow. (c) Reconstructed January–April Baker River streamflow and reconstructed SAM-Marshall (Villalba et al., 2012) for the 1765–2004 period. (d) Baker River streamflow and SAM-Marshall tree-ring reconstructions with a 25 year spline to emphasize the correlation between the low-frequency of both records. Both series have been detrended to remove their linear tendency. Pearson correlation r in parentheses were calculated from pre-whitened series. Significance p levels are: *0.05, **0.01, ***0.001.

(35°S) is correlated with the Annual instrumental-based reconstructed SAM ($r = -0.32$, $p < 0.05$, 1887–2000, Urrutia et al., 2011).

Similarly, the tree-ring based reconstructed spring – mid winter (October to June) streamflow of the Neuquén River located in Argentina at 38° 30′ and the annual SAM index are negatively correlated ($r = -0.384$, $p < 0.01$) over the 1887–2000 period (Mundo et al., 2012). The correlation between SAM and streamflow instrumental records for the 1957–2000 interval has been described for the Cautín River in Chile (38.5°S,) and the Chubut River in the Argentinean Andes (43.5°S, Villalba et al., 2012).

The positive deviations of the SAM indicate a southward shift of the Westerly winds storm tracks that bring precipitation (Thompson and Wallace, 2000). Consistently, re-analysis of ERA-40 and NCEP–NCAR data indicates that summer precipitation can be associated with circumpolar zonal flow anomalies at mid and high latitudes which are well correlated with hemispheric-scale SAM (Garreaud et al., 2013). This re-analysis also indicated a reduction of the westerlies in the 1968–2001 period over North-Central Patagonia (where the Baker basin is located) throughout the year, and especially during winter and spring, causing a drying trend (Garreaud et al., 2013).

The declining trend in the Baker streamflow since the 1980s is unprecedented in the entire 1765–2004 record and can be associated with reduced precipitation due to the increase in the SAM. A similar pattern has been described for the Puelo streamflow and to a lesser extent for the Maule River, located along the north–south hydroclimatic gradient at 41° 35′ and 35° 40′S, respectively (Lara et al., 2008; Urrutia et al., 2011).

There is a similar low-frequency variability pattern for the Baker discharge and the tree-ring reconstructed summer (December–February) SAM-Marshall (Villalba et al., 2012) during the 1765–2004 period ($r = -0.41$, $p < 0.01$) when both records are filtered with a 25-year spline and detrended (Fig. 8d). In the estimation of p no adjustment was made for the reduction of the degrees of freedom in the filtered series compared to the unfiltered ones. The main low-frequency common pattern is the steepest slope of opposite sign in both reconstructions starting in the mid 1980s (Fig. 8c and d and Villalba et al., 2012). It is highly relevant that the reconstructed SAM record was developed from tree-ring chronologies from over 3000 trees of the conifers *Austrocedrus chilensis* and *Araucaria araucana* from Central and Southern Chile and Argentina as well as other species from New Zealand and Tasmania. Therefore, it uses other species and chronologies and is completely independent from the Baker River reconstruction presented here that was developed from *N. pumilio*.

We analyzed the influence of El Niño Southern Oscillation (ENSO) on the reconstructed streamflow, and we found a negative correlation between discharge and current spring (October–November) and spring-summer (September-December) SOI index ($r = -0.46$ and -0.42, respectively, $p < 0.01$ in both cases, not shown). The predominance of SAM (AAO) as the main climatic driver of streamflow in Northern Chilean Patagonia with a lower influence of ENSO reported for the Baker River is consistent with the pattern described for the observed streamflow of the Puelo

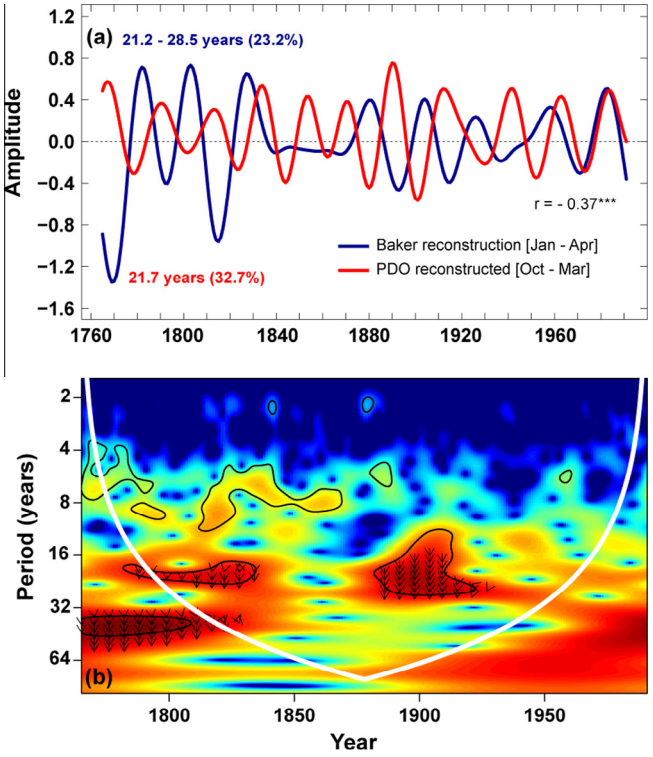

Fig. 9. (a) Comparison of decadal signals extracted by Singular Spectral Analysis (SSA) with the corresponding explained variance in percentage (%) for the Baker River streamflow and Pacific Decadal Oscillation (PDO) tree-ring reconstructions (Biondi et al., 2001). (b) Power amplitude co-spectral analysis of both records using Continuous Wavelet Transform with the timescale slightly displaced compared to panel (a). The thick black contours above the cone of influence designate the 95% confidence level against red noise. The arrows indicate amplitudes of contrary sign between both time series, indicating they are out of phase. Within the cone of influence, edge effects become important.

and Mañihuales, rivers located at 41° 40′S and 45° 30′S, respectively (Rubio-Álvarez and McPhee, 2010). This situation contrasts with that documented for Central and South Central Chile (35° – 37° 30′S) in which austral winter ENSO is the main driver of annual streamflow (Rubio-Álvarez and McPhee, 2010). The Maule reconstructed streamflow is also mainly correlated with ENSO (Urrutia et al., 2008).

We also investigated the potential effect of the Pacific Decadal Oscillation (PDO) as a climatic driver of the Baker River streamflow. The Singular spectrum amplitude of both the streamflow reconstruction and the reconstructed PDO (Biondi et al., 2001) have a similar pattern regarding their waveforms with periods of 21.2 – 28.5 years and 21.7- year cycles, which explain 23.2% and 32.7% of the total variance in each time series, respectively (Fig. 9a). Oscillations centered in these waveforms for both the streamflow and the PDO reconstructions are significantly correlated ($r = -0.37$ $p < 0.01$). In the estimation of p no adjustment was made for the reduction of the degrees of freedom in the filtered series compared to the unfiltered ones. The cross wavelet analysis shows coherency between both time series that are statistically significant ($p < 0.05$) especially around 8-year cycles in the 1810–1860 that are in phase (Fig. 9b). Longer wavelengths that are coherent between the streamflow and the PDO with cycles around 20-year and 12–30 years are dominant between 1810–1840 and 1880–1920, respectively, (Fig. 9b). Nevertheless, the amplitude of both records in these waveforms and periods has an opposite sign indicating that they are out of phase (Fig. 9a and b). Rubio-Álvarez and McPhee, 2010 also found significant negative correlation between summer streamflow and annual, winter and summer PDO for the rivers located between 37° 30′S and 41° 40′S, and annual and winter PDO for Mañihuales River (45° 30′S).

4. Conclusions

The Baker River has the highest mean discharge of rivers draining both slopes of the Andes South of 20°S and is among the six rivers with the highest mean streamflow in the Pacific domain of South America (1100 m^3 s^{-1} at its outlet). It drains a basin shared between Chile and Argentina with an area of 29,000 km^2, and it is internationally renowned for its great ecologic and economic present and future value, which includes conservation, tourism, recreational fishing, and hydropower. The hydropower potential includes two planned dams for the generation of a total of 1020 Mw/h. The dams have been highly controversial, and the future of this project is uncertain.

Despite the high relevance of the Baker River and basin, the scarcity, shortness and location of both precipitation and streamflow gauges, lack of snow accumulation, radiation and other climate records as well as the absence of available tree-ring reconstructions hampers the planning and decision making regarding water and other natural resources in the region. These limitations are magnified by the complex hydrological processes of the Baker basin characterized by strong precipitation gradients, presence of different land use-land cover types, diverse sources of runoff (rain, snow and glacier melt), as well as storage in large lakes (Dussaillant et al., 2012, Krögh et al., 2014).

This study reconstructs the austral summer – early fall (January-April) streamflow for the Baker River from tree-rings for the period 1765–2004. Summer streamflow contributes 45.2% of the annual discharge. This reconstruction constitutes the southern most tree-ring streamflow record worldwide (47° 30′S), and expands by 650 km the range of the hydroclimate gradient along South America covered by such records.

The reconstruction was based on principal components extracted from *N. pumilio* tree-ring composite chronologies developed from a total of 566 radii that are sensitive to precipitation and temperature. The regression model for the period (1961–2004) indicates robust statistics and explains 54% of the variance of the Baker River streamflow ($R^2_{adj} = 0.54$, compared to $R^2_{adj} = 0.42$ and 0.43 for the streamflow reconstruction of the Puelo and Maule Rivers in Chile, respectively, Lara et al., 2008; Urrutia et al., 2011).

The reconstruction of the Baker River streamflow reveals that the most significant temporal pattern in the record is the sustained decline since the 1980s ($\tau = -0.633$, $p = 1.0144 * 10^{-5}$ for the 1985–2004 period), which is unprecedented since 1765. This is the only 25-year period of reconstructed streamflow with a significant trend of any sign. The decreasing trend after the 1980s is also evident in the summer to early fall (January to April) and annual streamflow (not shown) instrumental records after 1980 (both series significantly correlated, $r = 0.71$, $p < 0.0001$).

Results of this study revealed two periods of below the mean reconstructed streamflow (1766–1775 and 1809–1818) that coincide with negative amplitudes for a cycle of 21.2 – 28.5 years, the dominant waveform in the record explaining 23% of the variance. An interesting temporal pattern is that three out of the five summers with the highest streamflows in the entire reconstructed record (1977, 1958, 1959) have occurred in the last decades. Conversely, only one year among the five with lowest reconstructed records occurred after the 1950s (2000) and occupies the fourth place in the ranking of low records. The causes of the extreme high values are not yet clear. The 1977 event may be associated with high precipitation in the previous April-September that might be an indication of snow accumulation in the previous fall to spring season combined with above maximum mean summer temperatures causing snow melt. Dated GLOF events could not be discerned in the monthly discharge records or summer records used in our study. Therefore, the causes of the occurrence of recent extreme high summer flows in the reconstructed record remain unclear.

Baker streamflow is positively correlated with previous fall to spring precipitation as an indication of snow accumulation, and also to precipitation and maximum temperature in the current summer, the latter explaining increased snowmelt. Nevertheless, inadequate coverage of precipitation gauges regarding their number and location limited to low elevations, as well as lack of snow records and strong winds lead to the underestimation of precipitation in the Baker basin and limits the understanding of the relationship of both tree-growth and streamflow with precipitation and temperature. A recent study based on hydrological modeling documents that infiltration accounts for 73% of total precipitation, and therefore soil storage becomes an important component of the hydrologic cycle (Krögh et al., 2014). Precipitation (both rain and snow melt) stored in the soil would favor both tree-growth and slower runoff with interflow as an important component, improving the understanding of the relationship between tree-growth and streamflow.

The recent decreasing trend in the reconstructed Baker River summer - early fall discharge as well as in regional precipitation that we document might be explained by the increase of the Southern Annular Mode (SAM), which is the main climatic forcing in Southern South America and has caused reduced precipitation over the region (Villalba et al., 2012). This is indicated by the correlation of the Baker reconstructed discharge with the November–April SAM-Marshall ($r = -0.55$, $p < 0.001$, 1961–2004). The reduction of streamflow associated with an increase in SAM in the last decades has also been described for the Puelo River (41° 35′S) and to a lesser extent for the Maule River (35° 40′S) reconstructions (Lara et al., 2008; Urrutia et al., 2011). These similar patterns occur despite the dramatic variation in climate, from sub-humid Mediterranean type to rainy oceanic climates (1000 to > 5000 and up to 10,000 mm of annual precipitation), encompassing pluvial to

mixed and snowmelt hydrological regimes. Spring to Summer SOI index also influences the summer to fall Baker River reconstructed streamflow (September–December) ($r = -0.42$, $p < 0.01$).

A relevant finding of this study is the negative correlation between the Baker reconstruction and the SAM-Marshall reconstruction for the 1765–2004 period ($r = -0.41$, $p < 0.01$), when both records are filtered with a 25-year spline and detrended (Fig. 8d and Villalba et al., 2012). Moreover, their trends of opposite slope after the 1950s, are unprecedented in both records, covering the last 600 years in the case of the SAM-Marshall reconstruction (Villalba et al., 2012). It should be noticed that the SAM reconstructed from tree-ring chronologies from Argentina and Chile used species other than *N. pumilio* (i.e. *Austrocedrus chilensis* and *Araucaria araucana*, both conifers) as well as others from New Zealand and Tasmania. Therefore the streamflow reconstruction for the Baker River presented here and the SAM reconstruction are totally independent. This emphasizes the strength and geographic coverage of SAM as the main climatic driver for tree-growth, precipitation and streamflow over a large portion of Southern South America (35° – 55°S).

There are discrepancies in the trends of the Baker streamflow. We report a decreasing trend of the observed and reconstructed streamflow of the Baker River in the 1980–2004 period for the intermediate watershed, that is consistent with precipitation decrease associated with the Southern Annular Mode. This is also coherent with the slight atmospheric cooling at the upper North and South Patagonian Ice Fields as well as a small but insignificant increase in ice field Surface Mass Balance (SMB) for the period 1979–2012 (Lenaerts et al., 2014). Nevertheless, the decreasing trend of the Baker River streamflow that we report here contradicts the increase of summer streamflow (January–February–March) for a portion of the Baker River intermediate watershed in the 1994–2008 period described by Dussaillant et al. (2012). This trend would be explained by the increase in the discharge of the Nef River due to glacier melt caused by temperature increase (Dussaillant et al., 2012), consistent with a generalized glacier retreat and thinning process reported for the North Patagonian Ice Field (Aniya, 2007; Rivera et al., 2007).

Monitoring and research in the next years should provide a better understanding of the hydrological processes and the relative contribution of rain, snow and glacier melt on runoff of the Baker basin. These efforts will also document how runoff and storage partitioning is changing as a response to climate variability and its drivers and the impacts of these changes on the Baker River streamflow.

The reduction in the summer-early fall streamflow after 1980, the increase in the occurrence of high deviations since the 1950s as unprecedented patterns since 1765, and the reported increase in the frequency of GLOF events in the last years causing floods, should be considered in decisions regarding water resources in the Baker Basin in both Chile and Argentina. These variability patterns and the trends predicted by atmospheric circulation and climatic models may have consequences in the future socio-economic development of the region, limiting conservation and productive activities that highly depend on the Baker River streamflow, such as tourism, recreational fishing and hydropower generation, as well as restricting the compatibility among these activities.

Future research should consider additional tree-ring sites widely distributed over the Baker watershed that might increase the explained variance of the streamflow record. New tree-ring reconstructions for other watersheds would provide a better understanding of the long-term temporal and spatial patterns of streamflow variability and its climatic drivers. An important challenge is expanding these reconstructions to cover the last 1000 or more years using long-lived species such as *Fitzroya cupressoides* and *Pilgerodendron uviferum* that have provided climate reconstructions with a broad regional signal. The installation of weather, streamflow gauges and other monitoring stations along elevation and west to east gradients, as well as studying and modeling the complex hydrological processes in the highly relevant Baker basin are also necessary. This should be the basis for planning, policy design and decision making regarding water resources in the Baker basin.

Acknowledgements

This research was supported by FONDECYT Grants N° 1090479 and 1130410, the Center for Climate and Resilience Research (CR)^2 funded by CONICYT/FONDAP/15110009, the IAI grant CRNII 2047b, and CONICYT 781301007. Alvaro González-Reyes thanks the Advanced Mining Technology Center (AMTC) of FCFM Universidad de Chile for a doctoral grant. We thank Dirección General de Aguas (DGA) and Dirección Meteorológica de Chile (DMC) for providing the instrumental data; Corporación Nacional Forestal (CONAF) and Parque Patagonia for permission to collect samples; Javier Godoy, Juan Carlos Llancabure, Natalia Riquelme, and Claudia Guerrido for fieldwork assistance. Carmen. G. Rodríguez and Marcela Valderas for chronology development. Sebastián Krögh, Maria P. Peña and Paulina Puchi for treatment and analysis of streamflow and meteorological data. Ricardo Villalba and Rocío Urrutia contributed to the development of the reconstruction. Aldo Farías drew the location map. We thank S. Krögh and James McPhee for their advise on the hydrological processes, and to two anonymous reviewers that contributed in improving this paper. This paper is a tribute to the Baker River and its long-term conservation.

Appendix A. Supplementary material

Supplementary data associated with this article can be found, in the online version, at http://dx.doi.org/10.1016/j.jhydrol.2014.12.007.

References

Aniya, M., 2007. Glacier variations of Hielo Patagónico Norte, Chile. Bull. Glacier Res. 24, 59–70.

Aravena, J.C., Lara, A., Wolodarsky-Franke, A., Villalba, R., Cuq, E., 2002. Tree-ring growth patterns and temperature reconstruction from *Nothofagus pumilio* (Fagaceae) forests at the upper tree line of Southern Chilean Patagonia. Rev. Chil. Hist. Nat. 75, 361–376.

Aravena, J.C., Luckman, B.H., 2009. Spatio-temporal rainfall patterns in southern South America. Int. J. Climatol. 29, 2106–2120. http://dx.doi.org/10.1002/joc.1761.

Arnell, N., Liu, C., Compagnucci, R., Da Cunha, L., Hanaki, K., Howe, C., Mailu, G., Shiklomanov, I., Stakhiv, E., 2001. Chapter 4. Hydrology and water resources. Climate Change 2001. Impacts, Adaptation, and Vulnerability. IPCC. Cambridge University Press, pp. 193–233.

Biondi, F., Gershunov, A., Cayan, R., 2001. North Pacific decadal climatic variability since 1661. J. Climate Lett. 14, 5–10.

Blasing, T.J., Solomon, A.M., Duvick, D.N., 1984. Response functions revisited. Tree-Ring Bull. 44, 1–17.

Briffa, K.R., 1995. Interpreting high-resolution proxy climate data: the example of dendroclimatology. In: von Storch, H., Navarra, A. (Eds.), Analysis of Climate Variability, Applications of Statistical Techniques. Springer, Berlin, Heidelberg, New York, pp. 77–94.

Brito-Castillo, L., Díaz-Castro, S., Salinas-Zavala, C.A., Douglas, A.V., 2003. Reconstruction of long-term winter streamflow in the Gulf of California continental watershed. J. Hydrol. 278, 39–50.

Cobos, D.R., Boninsegna, J.A., 1983. Fluctuations of some glaciers in the upper Atuel River basin, Mendoza, Argentina. Quaternary South Am. Antarct. Peninsula 1, 61–82.

Cohn, T.A., Lins, H.F., 2005. Nature's style: naturally trendy. Geophys. Res. Lett. 32. http://dx.doi.org/10.1029/2005GL024476. Art. No. L23402.

CONAF, CONAMA, BIRF, U., Austral, P., Universidad Católica de Chile, Universidad Católica de Temuco, 1999. Catastro y Evaluación de Recursos Vegetacionales Nativos de Chile. Informe Nacional con Variables Ambientales. Corporación Nacional Forestal, Santiago, p. 88.

Cook, E.R., 1985. A time series analysis approach to tree-ring standardization. Dissertation. University of Arizona.

Cook, E.R., Peters, K., 1981. The smoothing spline: A new approach to standardizing forest interior ring-width series for dendroclimatic studies. Tree-Ring Bull. 41, 45–53.
Cook, E.R., Krusic, P.J., Holmes, R.H., Peters, K., 2007. Program ARSTAN, Version 41d, 2007. <www.ldeo.columbia.edu/tree-ring-laboratory>.
DGF (Departamento de Geofísica de la Universidad de Chile, CL), 2007. Estudio de Variabilidad Climática en Chile para el Siglo XXI. Cambios Climáticos Regionales para fines del siglo XXI obtenido mediante el modelo PRECIS. Santiago, Chile. Comisión Nacional del Medio Ambiente (CONAMA. CL). www.dgf.uchile.cl/PRECIS.
Dussaillant, A., Benito, G., Buytaert, W., Carling, P., Meier, C., Espinoza, F., 2009. Repeated glacial-lake outburst floods in Patagonia: an increasing hazard? Nat. Hazards 54, 469–481. http://dx.doi.org/10.1007/s11069-009-9479-8.
Dussaillant, A., Buytaert, W., Meier, C., Espinoza, F., 2012. Hydrological regime of remote catchments with extreme gradients under accelerated change: the Baker basin in Patagonia. Hydrol. Sci. J. 57 (8), 1530–1542. http://dx.doi.org/10.1080/02626667.2012.726993.
Fritts, H.C., 1976. Tree Rings and Climate. Academic Press, New York, 567.
Garreaud, R.D., Vuille, M., Compagnucci, R., Marengo, J., 2009. Present-day South American climate. Palaeogeogr. Palaeoclimatol. Palaeoecol. 281, 180–195.
Garreaud, R., Lopez, P., Minvielle, M., Rojas, M., 2013. Large-scale control on the Patagonian climate. J. Climate 26, 215–230. http://dx.doi.org/10.1175/JCLI-D-12-00001.1.
Gordon, G.A., Le Duc, S.K., 1981. Verification statistics for regression models. In: Am. Meteorol. Soc. (Ed.), Preprints Seventh Conference on Probability and Statistics in Atmospheric Sciences, Monterey, California, U.S.A., pp. 129–133.
Grinsted, A., Moore, J.C., Jevrejeva, S., 2004. Application of the cross wavelet transform and wavelet coherence to geophysical time series. Nonlinear Process. Geophys. 11, 561–566.
Hess, A., Iyer, H., Malm, W., 2001. Linear trend analysis: a comparison of methods. Atmos. Environ. 35, 5211–5222.
Holmes, R.L., 1983. Computer assisted quality control in tree-ring dating and measurement. Tree-Ring Bull. 43, 69–78.
Holmes, R.L., Stockton, C.W., La Marche, V.C., 1979. Extension of river flow records in Argentina from long tree-ring chronologies. Water-Resour. Bull. 15 (4), 1081–1085.
Intergovernmental Panel on Climate Change, 2001. Climate change. Watson, R.T. (Ed.), Synthesis Report. Intergovernmental Panel on Climate Change, IPCC. <www.grida.no/climate/ipcc.tar/>.
Jain, S., Woodhouse, C.A., Hoerling, M.P., 2002. Multidecadal streamflow regimes in the interior Western United States: implications for the vulnerability of water resources. Geophys. Res. Lett. 29, 2036–2039. http://dx.doi.org/10.1029/2001GL014278.
Kaplan, M.R., Ackert, R.P., Singer, B.S., Douglass, D.C., Kurz, M.D., 2004. Cosmogenic nuclide chronology of millennial-scale glacial advances during O-isotope stage 2 in Patagonia. Geol. Soc. Am. Bull. 116, 308–321.
Kendall, M.G., 1975. Rank Correlation Methods. Griffin, London.
Kistler, R., Kalnay, E., Collins, W., Saha, S., White, G., Woollen, J., Chelliah, M., Ebisuzaki, W., Kanamitsu, M., Kousky, V., Van den Dool, H., Jenne, R., Fiorino, M., 2001. The NCEP-NCAR 50-year reanalysis: monthly means CD-ROM and documentation. Bull. Am. Meteorol. Soc. 82, 247–267.
Koutsoyiannis, D., Montanari, A., 2007. Statistical analysis of hydroclimatic time series: uncertainty and insights. Water Resour. Res. 43, W05429. http://dx.doi.org/10.1029/2006WR005592.
Krögh, S.A., Pomeroy, J.W., McPhee, J., 2014. Physically based hydrological modelling using reanalysis data in Patagonia. J. Hydrometeorol.. http://dx.doi.org/10.1175/JHM-D-13-0178.1.
Lara, A., Soto, D., Armesto, J., Donoso, P., Wernli, C., Nahuelhual, L., Squeo, F. (Eds.), 2003. Componentes científicos clave para una política nacional sobre usos, servicios y conservación de los bosques nativos Chilenos. Universidad Austral de Chile. Iniciativa Científica Milenio de Mideplan. PDF version available in <http://www.forecos.cl>.
Lara, A., Villalba, R., Wolodarsky-Franke, A., Aravena, J.C., Luckmann, B.H., Cuq, E., 2005. Spatial and temporal variation in *Nothofagus pumilio* growth at tree line along its latitudinal range (35° 40′-55°S) in the Chilean Andes. J. Biogeogr. 32, 879–893.
Lara, A., Villalba, R., Urrutia, R., 2008. A 400-year tree-ring record of the Puelo river summer-fall streamflow in the Valdivian rainforest eco-region, Chile. Climatic Change 86 (3–4), 331–356. http://dx.doi.org/10.1007/s10584-007-9287-7.
Lenaerts, J., van den Broeke, M., van Wessem, J., van de Berg, J., 2014. Extreme precipitation and climate gradients in Patagonia revealed by high-resolution regional atmospheric climate modeling. J. Climate 27, 4607–4621. http://dx.doi.org/10.1175/JCLI-D-13-00579.1.
Mann, M.E., Lees, J., 1996. Robust estimation of background. Noise and signal detection in climatic time series. Climatic Change 33, 409–445.
Marshall, G.J., 2003. Trends in the southern annular mode from observations and reanalyses. J. Climate 16, 4134–4143.
Meko, D.M., 1997. Dendroclimatic reconstruction with time varying subsets of tree indices. J. Climate 10, 687–696.
Meko, D.M., Woodhouse, C.A., 2011. Application of streamflow reconstruction to water resources management. In: Hughes, M.K., Swetnam, T.W., Diaz, H.F (Eds.), Tree Rings and Climate: Progress and Prospects. Springer, pp. 231–261.
Meko, D.M., Woodhouse, C.A., Baisan, C.H., Knight, T., Lukas, J.J., Hughes, M.K., Salzer, M.W., 2007. Medieval drought in the upper Colorado River Basin. Geophys. Res. Lett. 34 (10), L10705. http://dx.doi.org/10.1029/2007GL029988.
Michaelsen, J., 1987. Cross-validation in statistical climate forecast models. J. Climate Appl. Meteorol. 26, 1589–1600.
Miller, A., 1976. The climate of Chile. In: Schwerdtfeger, W. (Ed.), World Survey of Climatology. Climates of Central and South America. Elsevier, Amsterdam, The Netherlands, pp. 113–131.
Montaño, M., Sanfeliu, T., 2008. Ecosistema Guayas (Ecuador). Medio ambiente y Sostenibilidad. Revista Tecnológica ESPOL 21 (1), 1–6.
Mundo, I.A., Masiokas, M.H., Villalba, R., Morales, M.S., Neukom, R., Le Quesne, C., Urrutia, R.B., Lara, A., 2012. Multi-century tree-ring based reconstruction of the Neuquen River streamflow, northern Patagonia, Argentina. Climate Past 8, 815–829.
Ostrom, C., 1990. Time Series Analysis: Regression Techniques. Quantitative Applications in the Social Sciences 07-009, second ed. Newbury Park, CA.
Pardo, S., 2008. Recursos hídricos compartidos y problemas transfronterizos. ¿Existen mecanismos de solución de conflictos entre Chile y Argentina? Memoria para optar al Grado de Licenciado en Ciencias Jurídicas y Sociales. Universidad Austral de Chile, Valdivia, p. 39.
Pezoa, L.S., 2003. Recopilación y análisis de la variación de las temperaturas (período 1965–2001) y las precipitaciones (período 1931–2001) a partir de la información de estaciones meteorológicas de Chile entre los 33° y 53° de latitud sur. Tesis Escuela de Ingeniería Forestal. Universidad Austral de Chile.
Pino, M., 1976. Reconocimiento geológico de los Departamentos Cochrane y Baker – Undécima Región – Aysén. Tesis de prueba para optar al título de Geólogo. Universidad de Chile, Facultad de Ciencias Físicas y Matemáticas Departamento de Geología.
Rivera, A., Benham, T., Casassa, G., Mabmer, J., Dowdeswell, J., 2007. Ice elevation and areal changes of glaciers from the Northern Patagonia Icefield, Chile. Global Planet. Change 59 (1–4), 126–137.
Robinson, W.J., Evans, R., 1980. A microcomputer-based tree-ring, measuring system. Tree-Ring Bull. 40, 59–64.
Rosenblüth, B.H., Fuenzalida-Ponce, H., Aceituno, P., 1997. Recent temperature variations in southern South America. Int. J. Climate 17, 1–17.
Rubio-Álvarez, E., McPhee, J., 2010. Patterns of spatial and temporal variability in streamflow records in south central Chile in the period 1952–2003. Water Resour. Res. 46, W05514. http://dx.doi.org/10.1029/2009WR007982.
Sánchez, F.D., García, M., Jaramillo, O., Verdugo, N., 2010. Agua Superficial: Caracterización y Análisis de la Oferta. In: Instituto Nacional de Hidrología y Medioambiente (Ed.), Estudio Nacional del agua 2010, pp. 54–110.
Stokes, M.A., Smiley, T.L., 1968. An Introduction to Tree-ring Dating. University of Arizona Press, Tucson, AZ.
Thompson, D., Wallace, J.M., 2000. Annular modes in the extratropical circulation. Part I: month-to-month variability. J. Climate 13, 1000–1016.
Thompson, D., Solomon, S., Kushner, P., England, M., Grise, K., Karoly, D., 2011. Signatures of the Antarctic ozone hole in Southern Hemisphere surface climate change. Nat. Geosci. 4, 741–749. http://dx.doi.org/10.1038/ngeo1296.
Torrence, C., Compo, G.P., 1998. A practical guide to wavelet analysis. Bull. Am. Meteorol. Soc. 79, 61–78. http://dx.doi.org/10.1175/15200477(1998)079<0061:APGTWA>2.0.CO;2.
Urrutia, R., Lara, A., Villalba, R., Christie, D., Le Quesne, C., Cuq, A., 2011. Multicentury tree ring reconstruction of annual streamflow for the Maule River Watershed in South Central Chile. Water Resour. Res.. http://dx.doi.org/10.1029/2010WR009562.
Vautard, R., Ghil, M., 1989. Singular spectrum analysis in nonlinear dynamics, with applications to paleoclimatic time series. Physica D 35, 395–424.
Villalba, R., D'Arrigo, R., Cook, E., Wiles, G., Jacoby, G.C., 2001. Decadal-scale climatic variability along the extratropical Western Coast of the Americas: evidences from tree-ring records. In: Markgraf, V. (Ed.), Interhemispheric Climate Linkages. Academic, San Diego, California, U.S.A, pp. 155–172.
Villalba, R., Lara, A., Boninsegna, J.A., Masiokas, M., Delgado, S., Aravena, J.C., Roig, F.A., Schmelter, A., Delgado, S., Wolodarsky, A., Ripalta, A., 2003. Large-scale temperature changes across the southern Andes: 20th century variations in the context of the past 400 years. Climatic Change 59, 177–232.
Villalba, R., Lara, A., Masiokas, M.H., Urrutia, R.B., Luckman, B.H., Marshall, G.J., Mundo, I.A., Christie, D.A., Cook, E.R., Neukom, R., Allen, K., Fenwick, P., Boninsegna, J.A., Srur, A.M., Morales, M.S., Araneo, D., Palmer, J.G., Cuq, E., Aravena, J.C., Holz, A., Le Quesne, C., 2012. Unusual Southern Hemisphere tree growth patterns induced by changes in the Southern Annular Mode. Nat. Geosci.. http://dx.doi.org/10.1038/NGEO1613.
Vince, G., 2009. Dams for Patagonia. Science 329 (5990), 382–385. http://dx.doi.org/10.1126/science.329.5990.382 (23 July 2010).
Viviroli, D., Weingartner, R., Messerli, B., 2003. Assessing the hydrological significance of the world's mountains. Mountain Res. Dev. 23 (1), 32–40.
Wigley, T.M.L., Briffa, K.R., Jones, P.D., 1984. On the average value of correlated time series, with applications in dendroclimatology and hydrometeorology. J. Appl. Meteorol. 23, 201–213.
Woodhouse, C.A., 2001. A tree-ring reconstruction of streamflow for the Colorado Front Range. J. Am. Water Res. Assoc. 37 (3), 561–569.
Woodhouse, C.A., Lukas, J., 2006. Multi-century tree-ring reconstructions of colorado streamflow for water resource planning. Climatic Change 78 (2–4), 293–315.